MULTI-PARAMETRIC CONSTRAINED OPTIMAL CONTROL OF A PNEUMATIC ARTIFICIAL MUSCLE

George Andrikopoulos[*], George Nikolakopoulos[#], Ioannis Arvanitakis[*], Stamatis Manesis[*]

[*]*University of Patras*
Electrical and Computer Engineering Department
Rio GR-26500, Greece
[#]*Luleå University of Technology*
Department of Electrical, Computer and Space Engineering
Luleå, Sweden 97187

Abstract: The Pneumatic Artificial Muscle (PAM) is a highly non-linear form of actuation that is characterized by a decrease in the actuating length when pressurized. Its non-linear nature and time-varying parameters cause difficulties in modelling their characteristics and designing controllers for high-performance positioning systems. In this article, the control problem of a PAM is considered. A constrained linear and PieceWise Affine (PWA) system model approximation is utilized and a controller composed of: a) a feedforward term regulating control input at specific setpoints, and b) a Constrained Finite Time Optimal Controller (CFTOC) handling any deviations from the system's equilibrium points is synthesized. Simulation studies are used to investigate the efficacy of the suggested controller.

Keywords: Pneumatic Artificial Muscle, Piecewise Affine System, Optimal Control, Constrained Control, Feedforward Control.

1. INTRODUCTION

Pneumatic Artificial Muscle (PAM) (Pierce, 1940; Warszawska, 1967), also known as the McKibben Artificial Muscle (Chou and Hannaford, 1996; Schulte, 1961), Pneumatic Muscle Actuator or Fluidic Muscle (Gaylord, 1958; Yarlott, 1972) is a tube–like actuator that, when pressurised, decreases in actuating length. The McKibben–muscle is the most utilized type of PAMs, invented in 1950s by Joseph L. McKibben and utilized as an orthotic appliance for polio patients (Nickel *et al*., 1963). PAMs are significantly light actuators that are characterized by smooth, accurate and fast response and also are able to produce a significant force when fully stretched.

PAM typically consists of a rubber tube wrapped inside double helix synthetic fiber netting at predetermined angle. Protective rubber coating surrounds the fiber wrapping and appropriate metal fittings are attached at each end. The Fluidic Muscle, a PAM like the one presented in Fig.1, differs from the classic McKibben PAM as it utilizes a combined integration of the inner tube and external shell to a single aramid-neoprene mesh. An extensive overview of the most significant PAM applications can be found in (Andrikopoulos, *et al.*, 2011).

Fig. 1. Pneumatic Artificial Muscle (PAM) during contraction (top) and relaxation (bottom).

PAMs highly nonlinear nature and time-varying parameters cause difficulties in modeling their behavior and designing controllers for high-

performance positioning systems. Thus, PAMs present a challenging modeling and control problem.

Mainly during the past five years, there has been a growing trend in utilizing linear optimal controllers that are computed in an offline manner, thus, avoiding the great computational load that nonlinear controllers require for their design and implementation. More specifically, optimal control of PieceWise Affine (PWA) systems is receiving the growing attention of the research community since PWA systems represent a powerful tool for approximating nonlinear systems (Bemporad *et al.*, 2002).

In this article, a constrained linear and PWA system model approximation, derived from the fundamental modeling for static and dynamic PAM performance, will be presented; while a controller composed of: a) a feedforward term regulating control input at specific setpoints, and b) a Constrained Finite Time Optimal Controller (CFTOC) handling any deviations from the system's equilibrium points, is synthesized. Multiple simulation studies are being presented to prove the efficacy of the suggested controller in the contraction positioning problem of a PAM. Finally the conclusions and issues for further research activities will be drawn.

2. PAM MODELING

2.1 Force Model.

McKibben (Gaylord, 1958; Schulte, 1961), first derived a force equation for the actuator with the double helically wound fiber shell.

In Fig. 2, the basic geometrical characteristics of PAM are presented, while the utilized variables are defined as: l is the tube length, d is the bladder diameter, b is the thread length, n is the number of thread turns and θ is the braid angle, i.e. the angle between the helical fiber element length and the longitudinal axis of the actuator (Schulte, 1961).

As shown in (1), tension F is described as linearly proportional to relative pressure P, i.e. the absolute internal gas pressure minus the environment pressure, and a monotonic function of braid angle θ, i.e. the angle between the helical fiber element length and the longitudinal axis of the actuator (Tondu and Lopez, 2000).

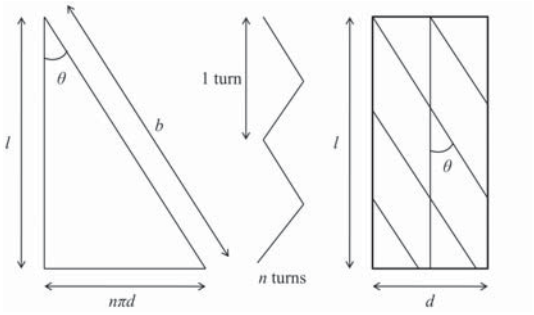

Fig. 2. Simplified geometrical model of PAM.

$$F = \frac{\pi d_0^2 P\left[3\cos^2\theta - 1\right]}{4} \qquad (1)$$

where d_0 is the diameter when θ=90°.

A similar geometric description of the PAM was utilized in (Tondu and Lopez, 2000) and another geometric model (2) was developed:

$$F = \pi\left(\frac{d_r}{2}\right)^2 P\left[a(1-\varepsilon)^2 - b\right] \qquad (2)$$

where $a = \frac{3}{\tan^2\theta_0}, b = \frac{1}{\sin^2\theta_0}, \varepsilon = \frac{l_0 - l}{l_0}$ and d_r, l_0, θ_0 are the initial diameter, initial nominal length, and the initial braid angle, respectively.

2.2 Dynamic Model.

During expansion, PAM experiences viscoelastic resistance which can be modeled as a damping and spring element. Thus, PAM is being considered as a parallel pattern that consists of a spring element, a damping element and a contractile element as presented in Fig. 3 (Reynolds, Repperger, Phillips, & Bandry, 2003). This model corresponds to a PAM placed on the vertical position with one end fixed and an external load L attached to the other end. The differential equation that describes the overall system is the following:

$$M\ddot{x} + D\dot{x} + Sx = F_{ce} - L \qquad (3)$$

where $x \in \Re^+$ is the displacement of the PAM, M is the mass of the muscle, P is the control pressure, L is the external load, S is the spring constant, D is the damping coefficient and F_{ce} is the contractile muscle force as shown in (2).

2.3 Piecewise Affine System Model Approximation.

The operating points x_j^{op}, with j={0,…,E} and $E \in \mathbb{Z}^+$, depend on the applied nominal pressures P_j^{op}, under the assumption of a constant load. Substituting (2) to (3) for $\ddot{x} = \dot{x} = 0$ yields:

$$P_j^{op} = \frac{Sx_j^{op} + L}{\pi r_0^2\left[a(1-\frac{x_j^{op}}{l_0})^2 - b\right]} \qquad (4)$$

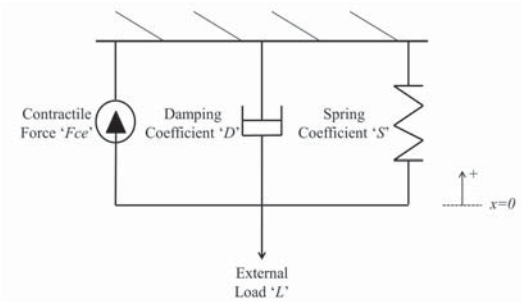

Fig. 3. Phenomenological dynamic model of PAM.

The linearized equations of motion for the PAM, around multiple equilibrium points j can be formulated by considering small perturbations around the variables x and P, or considering $x = x_j^{op} + \delta x$ and $P = P_j^{op} + \delta P$.

By applying this linearization approach in (3), it yields:

$$M\delta\ddot{x} + D\delta\dot{x} + Sx_j^{op} + S\delta x = F_{ce}(P_j^{op} + \delta P, x_j^{op} + \delta x) - L \quad (5)$$

Considering the Taylor expansion of (2) around the operating points:

$$\begin{aligned} F_{ce}(P_j^{op} + \delta P, x_j^{op} + \delta x) &= \pi r_0^2 P_j^{op}\left[a(1-\frac{x_j^{op}}{l_0})^2 - b\right] + \\ \pi r_0^2\left[a(1-\frac{x_j^{op}}{l_0})^2 - b\right]\delta P &- \pi r_0^2 P_j^{op}\left[\frac{2a}{l_0}(1-\frac{x_j^{op}}{l_0}) - b\right]\delta x \end{aligned} \quad (6)$$

and substituting (4) to (6) yields:

$$\begin{aligned} F_{ce}(P_j^{op} + \delta P, x_j^{op} + \delta x) &= \left(Sx_j^{op} + L\right) + \\ \pi r_0^2\left[a(1-\frac{x_j^{op}}{l_0})^2 - b\right]\delta P &- \frac{\left(Sx_j^{op} + L\right)\left[\frac{2a}{l_0}(1-\frac{x_j^{op}}{l_0})\right]}{\left[a(1-\frac{x_j^{op}}{l_0})^2 - b\right]}\delta x \end{aligned} \quad (7)$$

Inserting the expression from (7) to (5) is being obtained:

$$M\delta\ddot{x} + D\delta\dot{x} + Q\delta x = R\delta P \quad (8)$$

where $Q = S + \frac{\left(Sx_j^{op} + L\right)}{\left[a(1-\frac{x_j^{op}}{l_0})^2 - b\right]}\left[\frac{2a}{l_0}(1-\frac{x_j^{op}}{l_0})\right]$,

which by taking (3) into account becomes $Q = S + P_j^{op}\pi r_0^2\left[\frac{2a}{l_0}(1-\frac{x_j^{op}}{l_0})\right]$, and $R = \pi r_0^2\left[a(1-\frac{x_j^{op}}{l_0})^2 - b\right]$.

Addition of term $M\ddot{x}_j^{op} + D\dot{x}_j^{op} + Qx_j^{op}$ on both sides of (8) yields:

$$M\ddot{x} + D\dot{x} + Qx = Qx_j^{op} + R\delta P \quad (9)$$

The previous equation can be written as:

$$\ddot{x} + \frac{D_j}{M}\dot{x} + \frac{Q_j}{M}x = \frac{Q_j}{M}x_j^{op} + \frac{R_j}{M}\delta P \quad (10)$$

where the j^{th} subscript was used to denote the dependence of the previous variables on the selected operating point.

The equivalent state space models, accounting for small perturbations around the operating point x_j^{op}, are described as:

$$\begin{bmatrix}\dot{x}\\ \ddot{x}\end{bmatrix} = \begin{bmatrix}0 & 1\\ -\frac{Q_j}{M} & -\frac{D_j}{M}\end{bmatrix}\begin{bmatrix}x\\ \dot{x}\end{bmatrix} + \begin{bmatrix}0\\ \frac{R_j}{M}\end{bmatrix}\delta P + \begin{bmatrix}0\\ \frac{Q_j}{M}x_j^{op}\end{bmatrix} \quad (11)$$

or in an equivalent compact state space representation as:

$$\begin{aligned} \dot{\mathbf{x}} &= \mathbf{A_j}\mathbf{x} + \mathbf{B_j}\delta P + \mathbf{f_j} \\ \mathbf{y} &= \mathbf{C_j}\mathbf{x} + \mathbf{D_j}\delta P \end{aligned} \quad (12)$$

where $\mathbf{A_j} = \begin{bmatrix}0 & 1\\ -\frac{S_j}{M} - \frac{2\pi r_0^2 a}{Ml_0}P_j^{op}\left(1-\frac{x_j^{op}}{l_0}\right) & -\frac{D_j}{M}\end{bmatrix}$,

$\mathbf{B_j} = \begin{bmatrix}0\\ \frac{\pi r_0^2}{M}\left[a(1-\frac{x_j^{op}}{l_0})^2 - b\right]\end{bmatrix}$,

$\mathbf{C_j} = \begin{bmatrix}1 & 0\\ 0 & 1\end{bmatrix}$, $\mathbf{D_j} = \begin{bmatrix}0\\ 0\end{bmatrix}$,

$\mathbf{f_j} = \begin{bmatrix}0\\ \left[\frac{S_j}{M} + \frac{2\pi r_0^2 a}{Ml_0}P_j^{op}\left(1-\frac{x_j^{op}}{l_0}\right)\right]x_j^{op}\end{bmatrix}$,

$\mathbf{x} = \begin{bmatrix}x\\ \dot{x}\end{bmatrix} \in X \subseteq \mathbb{R}^2$ and $\delta P \in P \subseteq \mathbb{R}$, with the sets X and P to specify state and input operating regions that contain the operating points in their interior.

The system described in (11) is switched, as j belongs to a finite set of indexes and N denotes the number of switched systems, with the state x to act as the switching rule. If Σ is the polytope that contains all the switching systems, defined by the switching vertices $[\mathbf{A_j}, \mathbf{B_j}]$, it can be notated as:

$$\mathrm{Co}\{[\mathbf{A}_1, \mathbf{B}_1], ..., \mathbf{A}_L, \mathbf{B}_L\} \quad (13)$$

where the notation Co denotes the convex hull of the set.

These linear time-invariant state space models can be transformed into their discrete equivalents under the assumption of a sampling process with sampling period T_s. The discrete models can be cast in a compact form as a set of PWA subsystems:

$$\begin{aligned} \mathbf{x}(k+1) &= \mathbf{A_j^*}\mathbf{x}(k) + \mathbf{B_j^*}\delta P(k) + \mathbf{f_j^*} \\ \mathbf{y}(k) &= \mathbf{C_j^*}x(k) + \mathbf{D_j^*}\delta P(k) \end{aligned} \quad (14)$$

where $\begin{bmatrix}\mathbf{x}(k)\\ \delta P(k)\end{bmatrix} \in \Omega_i$ and Ω_i is a polyhedral partition of the state-input space over which the different dynamics are active.

3. CONSTRAINED FINITE TIME OPTIMAL CONTROLLER DESIGN

Consider the discrete time constrained Piecewise-Affine system described by (14). The number of subsystems involved in the adopted notation depends on the granularity of the selected equilibrium points $j = \{0, ..., E\}$.

Different segments of the polyhedral partitions are defined using constraints on state and input variables.

Let the state vector and control effort be constrained within certain regions (guard functions), or:

$$\begin{bmatrix} \mathbf{x}(k) \\ \delta P(k) \end{bmatrix} \in \Omega = \mathbf{H_j x} + \mathbf{J_j} \delta P \qquad (15)$$

which means that the *j* dynamics represented by the tuple $\left[\mathbf{A_j^*}, \mathbf{B_j^*}, \mathbf{f_j^*}, \mathbf{C_j^*}, \mathbf{D_j^*}\right]$, will be active in the part of state-input space which satisfies the constraints in (15). The same equation partitions the $(P \times X) \subseteq R^3$ space into a set of polyhedral Ω.

The controller's objective is to compute a cost-optimal solution that generates the additional stabilizing $\delta P(k)$ control effort by minimizing a quadratic cost objective over a receding horizon as:

$$\delta P(k) = \min_{\delta P(0),..,\delta P(N-1)} \Big[\mathbf{x}(N)^T \mathbf{W} \mathbf{x}(N) + \sum_{i=0}^{N-1} \begin{pmatrix} \delta P(k)^T U \delta P(k) + \mathbf{x}(k)^T \mathbf{V} \mathbf{x}(k) + \\ (\mathbf{y}(k) - \mathbf{y}_{ref})^T \mathbf{V_y} (\mathbf{y}(k) - \mathbf{y}_{ref}) \end{pmatrix} \Big] \qquad (16)$$

where *N* is the prediction horizon interval, **V**, $\mathbf{V_y}$, *U*, and **W** are the weighting matrices on the states, the outputs, the control effort and the terminal state, respectively.

This Constrained Finite Time Optimal Controller (CFTOC) is computed (Bemporad et al., 2002; Kvasnica *et al.*, 2004) as a piecewise affine feedback control of the following form:

$$\delta P = \mathbf{F}_j \mathbf{x}(k) + \mathbf{G}_j \text{ , if } \mathbf{x}(k) \in \Omega_j \qquad (17)$$

where Ω_j is the *j*-th active polyhedral spanning the space affected by the prediction horizon *N*, the guard functions defined in (15) and the parameters *U*, *V*, *W*, and *x(k + N)* involved in the formulation of the cost function in (16).

The overall control framework appears in Fig. 3, where it is shown that the suggested controller consists of: 1) a feedforward portion generating the control effort P_o based on the desired position x_{ref}, and 2) the multi parametric controller generating the deviation *δP* to account for any perturbations along the nominal desired position.

It should be noted that the calculation of the *δP(k)* control effort is being performed in an off line manner, and thus the presented approach is ideal for the real-time implementation of the proposed control scheme. Furthermore, the number of computed polyhedral depends on the length of the prediction horizon *N* and the nature of the guard functions.

In multi-parametric approaches, despite the offline computation of a feedback law, the exponential number of transitions between regions, which can occur when a controller is computed in a dynamic programming fashion, is the main reason why such high complexity programs can become prohibitive for larger problems (Borrelli *et al.*, 2003).

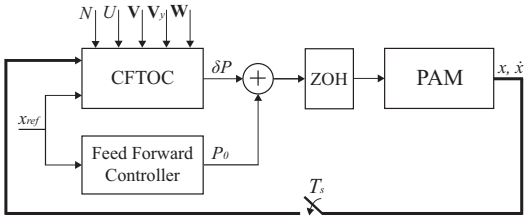

Fig. 3. Feedforward and Multi-parametric Feedback Control Framework.

4. SIMULATION RESULTS

Simulation studies were carried on a Festo MXAM–40–AA–DMSP–40–305N–AM–CM Fluidic Muscle with 40mm of internal diameter, 305mm of nominal length, 840g of mass and allowable displacement of $x \in [0, 91]$mm . The PAM is on the vertical position and has its upper end clumped. With no additional load attached to the PAM, half of its mass *M* is supported; the *L* load is constant and equals half the weight of the PAM.

For the optimal estimation of the damping *D* and spring *S* coefficients of (3), extensive experimental contraction studies were conducted. The specific stages of the experimental procedure are described in detail in (Andrikopoulos *et al.*, 2012).

Having estimated the relations of *S(P)* and *D(P)*, under the assumption of a constant *L*, the total number of PWA subsystems has been properly selected as *E*=6, which corresponds to 6 linearization points. Based on the assumption of linear relationships of *S(P)* and *D(P)* in an operating region, the aforementioned coefficient values, as well as the operating parameters and their respective regions, are presented in Table 1.

Table 1 PAM PWA operating points, operating subsystem regions and their respective spring and damping coefficient values

E	*Operating Points [m, m/s]*	*Operating Regions [m]*	*S*	*D*
1	$\mathbf{x}^{op} = [0.0166, 0]$	$x \in [0, 0.0406]$	19400	13192
2	$\mathbf{x}^{op} = [0.0590, 0]$	$x \in [0.0406, 0.0692]$	15633	9726
3	$\mathbf{x}^{op} = [0.0752, 0]$	$x \in [0.0692, 0.0795]$	12883	6344
4	$\mathbf{x}^{op} = [0.0827, 0]$	$x \in [0.0795, 0.0851]$	13017	5384
5	$\mathbf{x}^{op} = [0.0869, 0]$	$x \in [0.0851, 0.0884]$	13633	5114
6	$\mathbf{x}^{op} = [0.0899, 0]$	$x \in [0.0884, 0.0911]$	14300	5195

The operating regions' boundary elements are selected as the steady state values of the PAM system open loop response for pressures from 0 to 600kPa, in intervals of 100kPa; whereas their respective linearization points are selected as the steady state values of the PAM system open loop response for the middle-point pressures P^{op} from 50 to 550kPa, with 100kPa intervals.

Each linearized PWA subsystem is valid in only one of these regions. Therefore the guard functions for x_j in the *j*-th operating region are the corresponding

boundaries of the region. In these simulation studies, no constraint is posed on the state velocity $\dot{x}$, while the control feedback effort has been constrained, having a guard function of $-100 \le \delta P \le 100$ (kPa).

The goal of the controller is to solve the setpoint problem which drives all outputs towards the desired ones (set-point regulation). The parameters involved in the quadratic cost objective (16) were set to $\mathbf{V} = \mathbf{V}_y = 10^6 \mathbf{I}_{2\times 2}$, $U = 10^{-4}$, and $\mathbf{W} = \mathbf{0}_{2\times 2}$. The number of controller regions and polyhedral involved in the partitioning of the $[x, \dot{x}]$ space with respect to the prediction horizon $N = 1,...,5$ appears in Fig. 4.

An increase in the prediction horizon *N* results in a significant increase to the number of polyhedral partitions and an overall smoother response of the closed loop simulated PAM system. As shown in Fig. 5, for *N*=3 the space is partitioned into 135 regions. The respective generated feedback control effort for the same prediction horizon appears in Fig. 6. Figure 7 displays the 570-polyhedra for the same cost objective parameters and *N*=5.

The step response of the nonlinear simulated PAM system for *N=3,* initial states of $\mathbf{x}_{\text{initial}} = [0,0]$ and desired states of $\mathbf{x}_{\text{ref}} = [0.06,0]$, is shown in Fig. 8; while in Fig. 9 the overall control effort $P = P_0\big|_{x_{\text{ref}}=0.06} + \delta P$ is displayed. The response is characterized by rapid convergence, absence of major state fluctuations and a total steady state error of 0.5%.

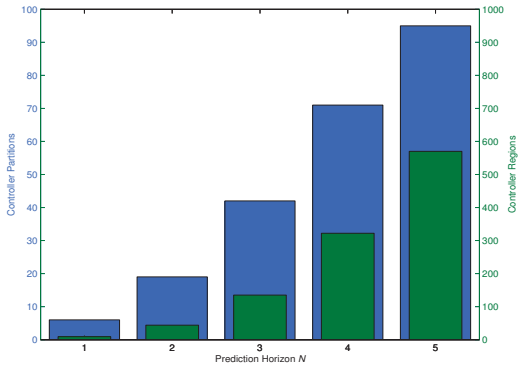

Fig. 4. Polyhedral partitioning with respect to prediction horizon *N*.

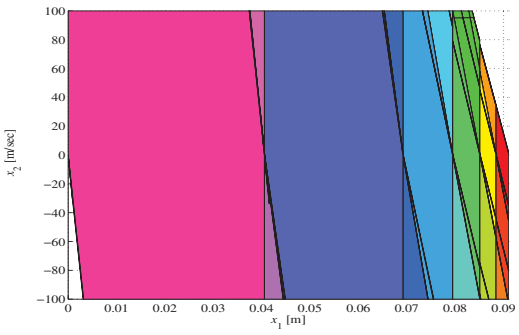

Fig. 5. Polyhedral Partition over 135 regions for *N=3*.

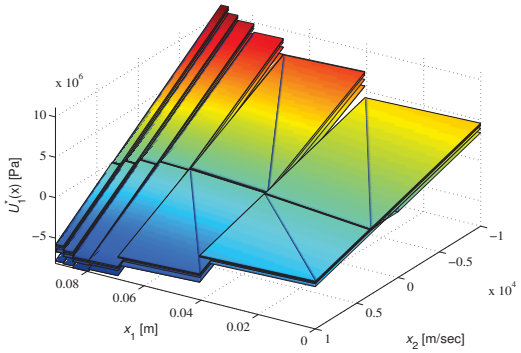

Fig. 6. Feedback Control Effort for *N=3*.

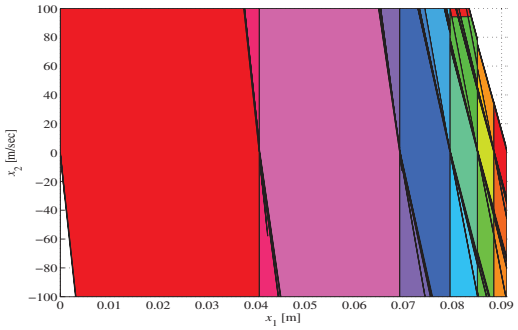

Fig. 7. Polyhedral Partition over 570 regions for *N=5*.

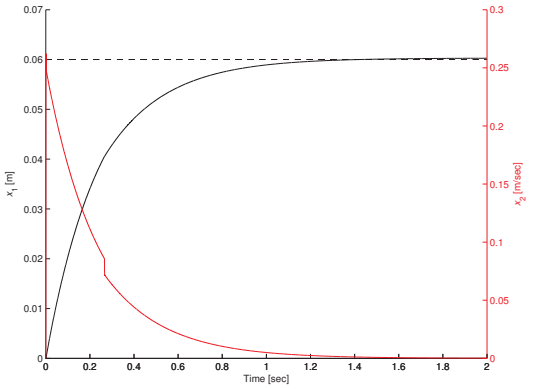

Fig. 8. PAM step response for *N*=3, $\mathbf{x}_{\text{initial}} = [0,0]$ and $\mathbf{x}_{\text{ref}} = [0.06,0]$.

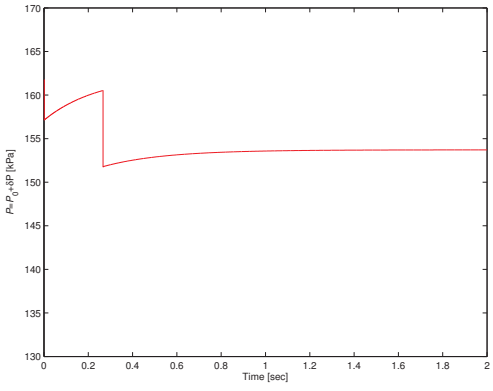

Fig. 9. Overall control effort *P* for step response with *N*=3, $\mathbf{x}_{\text{initial}} = [0,0]$ and $\mathbf{x}_{\text{ref}} = [0.06,0]$.

An additional step response of the nonlinear simulated PAM system is presented in Fig. 10, for *N=3,* initial states of $\mathbf{x}_{\text{initial}} = [0,0]$ and desired states of $\mathbf{x}_{\text{ref}} = [0.086,0]$. The respective overall control effort $P = P_0\big|_{x_{\text{ref}}=0.086} + \delta P$ is displayed in Fig. 11. The response is also characterized by rapid convergence (settling time less than 0.5 sec), absence of major state fluctuations and a total steady state error of 0.4%; thus, proving the efficacy of the proposed control scheme.

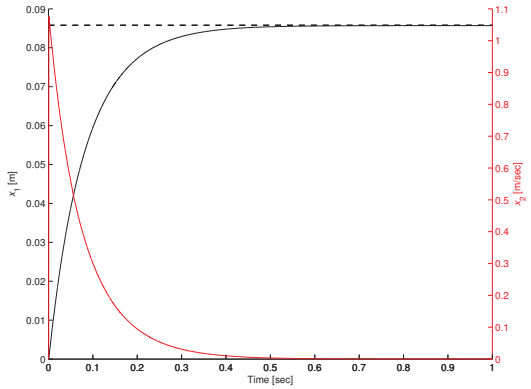

Fig. 10. PAM step response for *N*=3, $\mathbf{x}_{\text{initial}} = [0,0]$ and $\mathbf{x}_{\text{ref}} = [0.086,0]$.

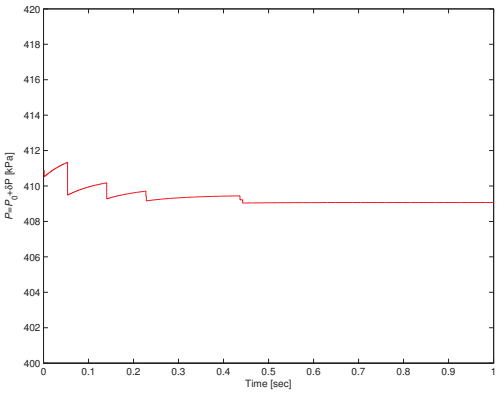

Fig. 11. Overall control effort *P* for step response with *N*=3, $\mathbf{x}_{\text{initial}} = [0,0]$ and $\mathbf{x}_{\text{ref}} = [0.086,0]$.

6. CONCLUSIONS

In this article, a constrained linear and PWA system model approximation, derived from the fundamental modeling for static and dynamic PAM performance, was presented. Moreover, a setpoint regulator was developed with the synthesis of: a) a feedforward term regulating control input at specific setpoints, and b) a Constrained Finite Time Optimal Controller (CFTOC) handling any deviations from the system's equilibrium points. Simulation studies were used to investigate and evaluate the efficacy of the suggested controller in the positioning problem of a PAM. The responses of the simulated nonlinear PAM system were characterized by rapid convergence, absence of major state fluctuations and a very small steady state error. Experimental evaluation of the controller's efficacy on a PAM testbed and utilization of the aforementioned control scheme on a larger scale PAM application are work in progress.

REFERENCES

Andrikopoulos, G., Arvanitakis, J., Nikolakopoulos, G., and Manesis, S. (2012). A Switched System Modeling Approach for a Pneumatic Muscle Actuator. IEEE International Conference on Industrial Technology (ICIT). Athens, Greece.

Andrikopoulos, G., Nikolakopoulos, G., and Stamatis Manesis. (2011). A Survey on applications of Pneumatic Artificial Muscles. Mediterranean Conference on Control and Automation (MED), pp. 1439-1446. Corfu, Greece.

Bemporad, Alberto, Morari, M., Dua, V., and Pistikopoulos, E. N. (2002). The explicit linear quadratic regulator for constrained systems. Automatica, 38, pp. 3-20.

Borrelli, F., Baotic, M., Bemporad, A., and Morari, M. (2003). An efficient algorithm for computing the state feedback optimal control law for discrete time hybrid systems. American Control Conference, Vol. 6, pp. 4717-4722.

Chou, C.-P., and Hannaford, B. (1996). Measurement and modeling of McKibben pneumatic artificial muscles. IEEE Transactions on Robotics and Automation, 12(1), pp. 90-102.

Gaylord, R. H. (1958). Fluid Actuated Motor System and Stroking Device. US Patent.

Kvasnica, M., Grieder, P., Morari, M., and M., B. (2004). Multi–Parametric Toolbox (MPT). Hybrid Systems: Computation and Control, 2993, pp. 448-462.

Nickel, V., Perry, J., and Garrett, A. (1963). Development of useful function in the severely paralyzed hand. Journal of Bone and Joint Surgery, 45-A(5), pp. 933–952.

Warszawska, P. (1967). Artificial Pneumatic Muscles. Dutch Patent.

Pierce, R. (1940). Expansible cover. U.S. Patent.

Reynolds, D. B., Repperger, D. W., Phillips, C. A., and Bandry, G. (2003). Modeling the Dynamic Characteristics of Pneumatic Muscle. Annals of Biomedical Engineering, 31(3), pp. 310-317.

Schulte, H. F. (1961). The characteristics of the McKibben artificial muscle. The Application of External Power in Prosthetics and Orthotics, pp. 94-115.

Tondu, B., and Lopez, P. (2000). Modeling and control of McKibben artificial muscle robot actuators. Control Systems Magazine, IEEE, 20(2), pp. 15–38.

Yarlott, J. (1972). Fluid actuator. US Patent.